Papers submitted to the Conference "Applications of Physics in Mechanical and Material Engineering"

The Influence of the Topology of Quasi One-Dimensional Structure on Frequency Distribution Inside Phononic Crystal

S. Garus[a,*], W. Sochacki[a], J. Garus[a] and J. Rzącki[b]

[a] *Department of Mechanics and Fundamentals of Machinery Design, Faculty of Mechanical Engineering and Computer Science, Częstochowa University of Technology, Dąbrowskiego 73, 42-201 Częstochowa, Poland*
[b] *Department of Physics, Faculty of Production Engineering and Materials Technology, Czestochowa University of Technology, ul. Dąbrowskiego 73, 42-201 Częstochowa, Poland*

Doi: 10.12693/APhysPolA.142.7 *e-mail: sebastian.garus@pcz.pl

In phononic crystals, for certain frequency ranges, the mechanical wave does not propagate. This phenomenon is called the occurrence of the phononic band gap and is related to the geometry of the structure, the spatial distribution of the materials and their type. The study analyzes the existence of a band gap inside quasi one-dimensional structures. The finite-difference time-domain algorithm and the transfer matrix method algorithm were used to simulate wave propagation in quasi-one-dimensional structures (i.e., those in which one dimension is much smaller than the other two). Then, the time series created inside the structure were subjected to signal decomposition into sinusoidal components of different frequencies using fast Fourier transform. The obtained results allowed to demonstrate the existence of a band gap in the structure and showed how the change in the distribution of layers affects the frequency range of the band gap.

topics: phononic crystal, FDTD, TMM, phononic band gap

1. Introduction

Quasi one-dimensional multilayer structures are a type of composite in which one of the dimensions is significantly smaller than the other two. They are used, inter alia, as filters for mechanical waves [1–5], but also as medical devices [6, 7], waveguides [8–10], acoustic barriers [11], sensors [12], acoustic diodes [13] or energy harvesting devices [14–16]. One of the most interesting phenomena occurring during wave propagation in multilayer structures is the presence of the phononic band gap (PhnBG) [17–21]. This phenomenon occurs when a wave of a given frequency does not propagate in the system. The presence of PhnBG is influenced by the types of materials used, the thickness of the layers and their distribution in the structure.

Using the transfer matrix method (TMM) of the algorithm, the distribution of mechanical wave transmission in a multilayer structure can be determined, and wave propagation can be studied using the finite difference time domain (FDTD) algorithm [22].

The study analyzed the effect of the arrangement of layers in a structure made of polylactic acid (PLA) immersed in water on the occurrence of band gaps for a mechanical wave in the range of acoustic frequencies. Then, for the selected structure, an analysis of the mechanical wave propagation inside the structure was carried out for the selected frequencies of the transmission peak and the band gap.

2. Layer distributions

In order to check the influence of the order of layer distribution on the occurrence and location of the band gaps, the transmission was determined for the next generations of the exemplary periodic (binary), quasi-periodic (Thue–Morse) and aperiodic (Severin) structures. These structures were selected in such a way that for each generation number L, the structures had the same number of plies and the same thickness (assuming the same thickness for each layer).

To create the binary X_L^{B} structure, the concatenation rule is used

$$X_L^{\mathrm{B}} = (\mathrm{AB})^{2^{L-1}}, \tag{1}$$

where the exponent 2^{L-1} defines the multiplicity of repetitions of the base element (AB) for a given generation L.

The quasi-periodic Thue–Morse structure of $X_L^{\mathrm{T-M}}$ is formed using the recursive substitution rule

$$\begin{cases} \mathrm{A} \to \mathrm{AB}, \\ \mathrm{B} \to \mathrm{BA}, \end{cases} \tag{2}$$

where the initial condition for this structure is

$$X_0^{\mathrm{T-M}} = \mathrm{A}. \tag{3}$$

The aperiodic structure of Severin X_L^{S}, like the Thue–Morse structure, is also created using the recursive substitution rule

$$\begin{cases} \mathrm{A} \to \mathrm{BB} \\ \mathrm{B} \to \mathrm{AB} \end{cases} \tag{4}$$

and the initial condition for the Severin structure was defined as

$$X_0^{\mathrm{S}} = \mathrm{B}. \tag{5}$$

The generation of an L structure for a recursive substitution rule means the multiple use of the rule in (2) and (4).

Table I shows the layer distribution for L generation numbers ranging from 2 to 5 for the X_L^{B}, Thue–Morse $X_L^{\mathrm{T-M}}$ and Severin X_L^{S} binary structures.

3. Transfer matrix method

In order to calculate the transmission of a mechanical wave through the multilayer structure, the structure characteristic matrix should be determined

$$M(f) = \frac{Z_1 + Z_{\mathrm{in}}}{2Z_i} \begin{pmatrix} 1 & \frac{Z_1 - Z_{\mathrm{in}}}{Z_1 + Z_{\mathrm{in}}} \\ \frac{Z_1 - Z_{\mathrm{in}}}{Z_1 + Z_{\mathrm{in}}} & 1 \end{pmatrix} \prod_{i=1}^{N-1} \left[\begin{pmatrix} \mathrm{e}^{\mathrm{i}\frac{2\pi f}{c_i} d_i} & 0 \\ 0 & \mathrm{e}^{-\mathrm{i}\frac{2\pi f}{c_i} d_i} \end{pmatrix} \frac{Z_{i+1} + Z_i}{2Z_{i+1}} \begin{pmatrix} 1 & \frac{Z_{i+1} - Z_i}{Z_{i+1} + Z_i} \\ \frac{Z_{i+1} - Z_i}{Z_{i+1} + Z_i} & 1 \end{pmatrix} \right]$$
$$\times \begin{pmatrix} \mathrm{e}^{\mathrm{i}\frac{2\pi f}{c_N} d_N} & 0 \\ 0 & \mathrm{e}^{-\mathrm{i}\frac{2\pi f}{c_N} d_N} \end{pmatrix} \frac{Z_{\mathrm{out}} + Z_N}{2Z_{\mathrm{out}}} \begin{pmatrix} 1 & \frac{Z_{\mathrm{out}} - Z_N}{Z_{\mathrm{out}} + Z_N} \\ \frac{Z_{\mathrm{out}} - Z_N}{Z_{\mathrm{out}} + Z_N} & 1 \end{pmatrix}, \tag{6}$$

where d_i is the thickness of the layer i. The acoustic impedance Z_i is determined from the product of the phase velocity c_i and the mass density ϱ_i according to

$$Z_i = c_i \varrho_i. \tag{7}$$

The transmission $T(f)$ for a given frequency f is determined by

$$T(f) = \left| \frac{1}{M_{11}(f)} \right|^2. \tag{8}$$

In order to investigate the effect of layer distribution, in these study lossless materials were analyzed, where material A was water ($c_{\mathrm{A}} = 1480$ m/s, $\varrho_{\mathrm{A}} = 1000$ kg/m^3) [23] and material B was PLA ($c_{\mathrm{B}} = 2220$ m/s, $\varrho_{\mathrm{B}} = 1240$ kg/m^3) [24]. The thickness of the layers was 2 cm. The analyzed structure was surrounded by water.

TABLE I

Layer distribution for the binary X_L^{B}, Thue–Morse $X_L^{\mathrm{T-M}}$ and Severin X_L^{S} structures for the L generation number values in the range from 2 to 5.

Structure	L			
	2	3	4	5
X_L^{B}	ABAB	ABABABAB	ABABABAB	ABABABAB
			ABABABAB	ABABABAB
				ABABABAB
$X_L^{\mathrm{T-M}}$	ABBA	ABBABAAB	ABBABAAB	ABBABAAB
			BAABABBA	BAABABBA
				ABBABAAB
				BAABABBA
X_L^{S}	BBAB	ABABBBAB	BBABBBAB	ABABBBAB
			ABABBBAB	ABABBBAB
				BBABBBAB
				ABABBBAB

4. The finite-difference time-domain algorithm

In order to study wave propagation in the FDTD algorithm, the system of

$$\frac{\partial P(\boldsymbol{x},t)}{\partial t} = \rho\, c^2 \nabla \boldsymbol{v}(\boldsymbol{x},t), \tag{9}$$

$$\rho \frac{\partial \boldsymbol{v}(\boldsymbol{x},t)}{\partial t} = \nabla P(\boldsymbol{x},t). \tag{10}$$

is used. The scalar pressure field $P(\boldsymbol{x},t)$ is dependent in time t and the space $\boldsymbol{x}$ on the vector velocity field $\boldsymbol{v}(\boldsymbol{x},t)$, and the medium where the mechanical wave propagates is described by the phase velocity c and the mass density ρ.

Let us transform (9) and (10) to one-dimensional form and assume a shift between pressure points and velocity-field points by half the space–time step, and then replace the derivatives with differences. We obtain the following form

$$P_k^{n+1/2} = P_k^{n+1/2} + \frac{\Delta t}{\Delta z} \rho_k\, c_k^2 \left(\boldsymbol{v}_{k+1/2}^n - \boldsymbol{v}_{k-1/2}^n \right), \tag{11}$$

$$\boldsymbol{v}_{k+1/2}^{n+1} = \boldsymbol{v}_{k+1/2}^n + \frac{\Delta t}{\Delta z\, \rho_k} \left(P_{k+1}^{n+1/2} - P_k^{n+1/2} \right). \tag{12}$$

In order to ensure the stability of the simulation, the Courant condition should be met, i.e.,

$$\Delta t \leq \frac{\Delta z}{c_{\max}}. \tag{13}$$

It links the step in time Δt and of the space Δz with the highest possible phase velocity $c_{\max}$ of a propagating mechanical wave. The algorithm uses a soft sound source and the transition from time domain to frequency domain was made using fast Fourier transform (FFT).

5. Results and discussion

Figures 1, 2 and 3 show the transmission as a function of frequency for the generation number $L = 2$–5 for the binary structures X_L^{B}, Thue–Morse $X_L^{\mathrm{T-M}}$ and Severin X_L^{S}, respectively. It was assumed in the study that the sound pressure level (SPL(A)) below 60 dB indicates the presence of band gaps, marked in gray on the graphs. The energy of the incident wave is actually reduced by 99.9% at the chosen level of 60 dB.

The research results presented in Fig. 1–3 show the occurrence of the phononic band gap phenomenon for some of the analyzed structures. For higher values of L and with less ordering of the structure, the band gap occurred for the lower frequency values. In the X_3^{B} binary structure, the gap was above 19.27 kHz. In X_4^{B}, the gap started from 18.11 kHz and for X_5^{B} it was from 18.14 kHz, however, the energy decrease was significantly lower for X_5^{B} than for X_4^{B}. For the Thue–Morse $X_4^{\mathrm{T-M}}$ structure there was one band gap of SPL(A)

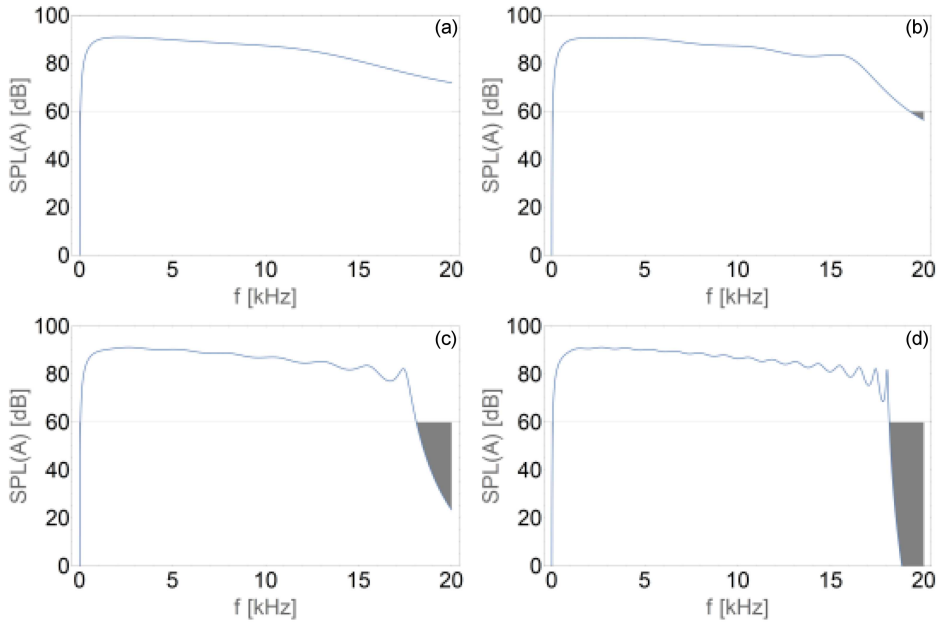

Fig. 1. Transmission for the binary structure with forbidden areas marked for (a) X_2^{B}, (b) X_3^{B}, (c) X_4^{B}, (d) X_5^{B}.

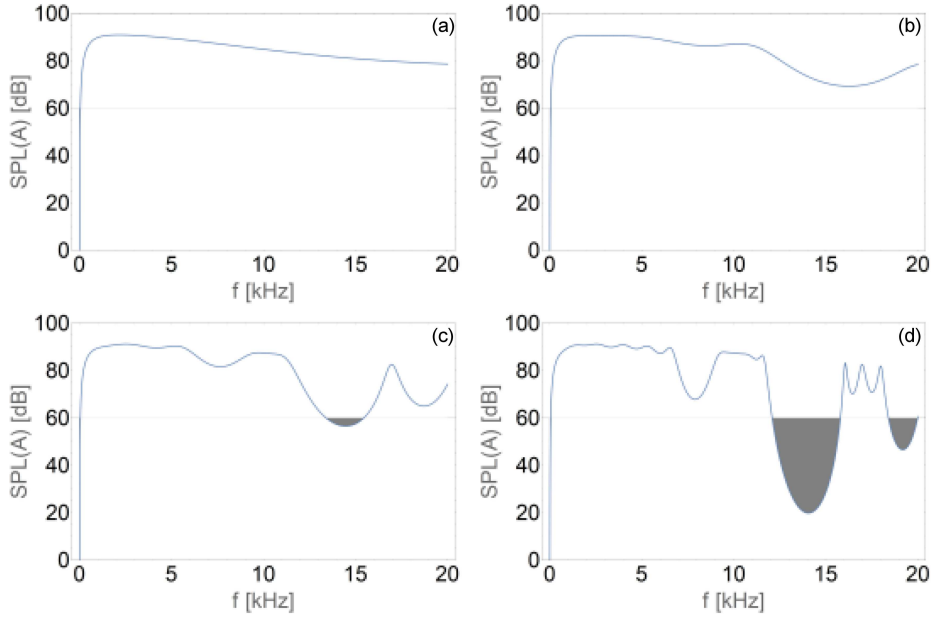

Fig. 2. Transmission for the Thue–Morse structure with the forbidden areas marked for (a) $X_2^{\mathrm{T-M}}$, (b) $X_3^{\mathrm{T-M}}$, (c) $X_4^{\mathrm{T-M}}$, (d) $X_5^{\mathrm{T-M}}$.

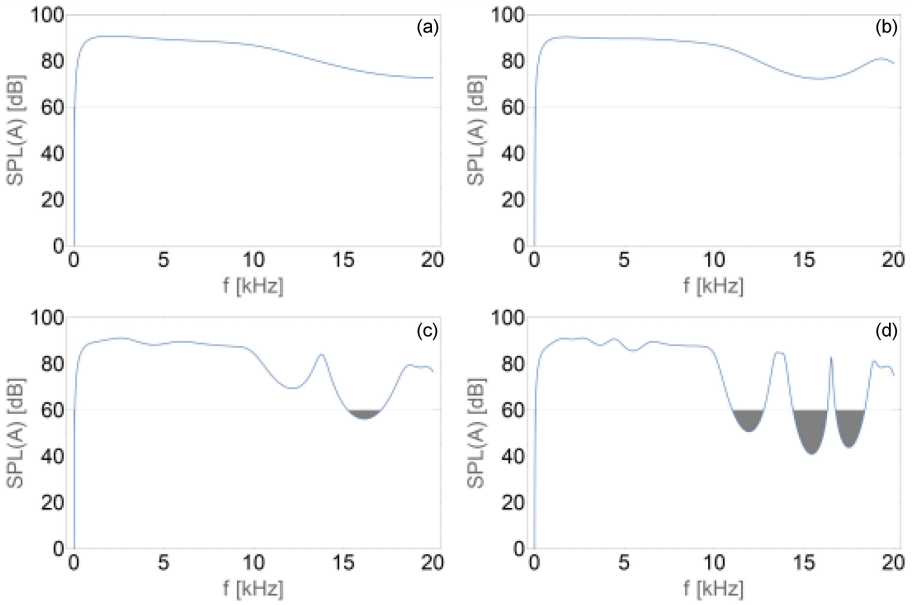

Fig. 3. Transmission for the Severin structure with the forbidden areas marked for (a) X_2^{S}, (b) X_3^{S}, (c) X_4^{S}, (d) X_5^{S}.

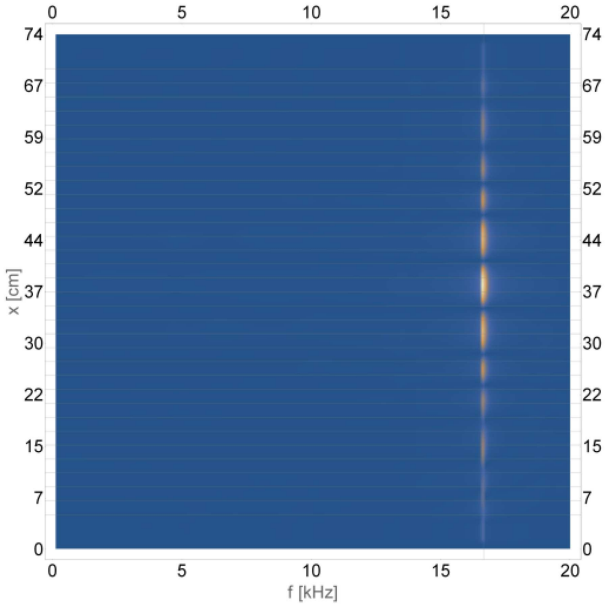

Fig. 4. The frequency distribution of the mechanical wave in the full acoustic spectrum for the frequency of the wave source of 16.5 kHz (high transmission peak).

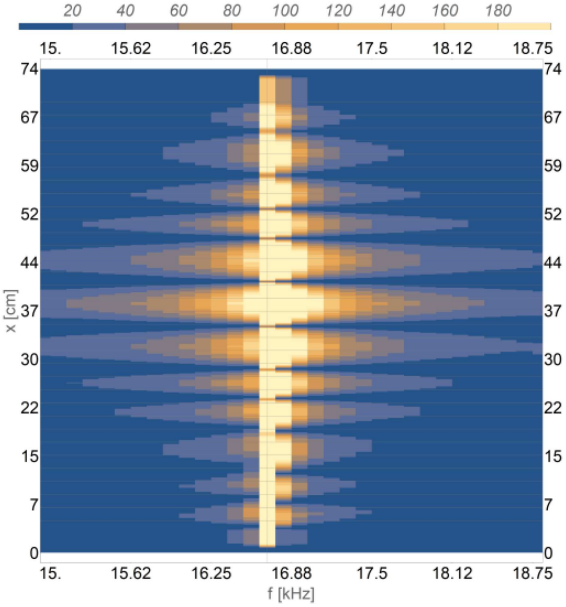

Fig. 5. The frequency distribution of the mechanical wave near the source frequency.

in the frequency range 13.41–15.45 kHz, while for the $X_5^{\mathrm{T-M}}$ structure there were two band gaps in the ranges 12.08–15.79 kHz and 18.4–19.98 kHz. For the Severin X_4^{S} structure, as for Thue–Morse $X_4^{\mathrm{T-M}}$, there was one band gap in the frequency range 15.26–17.09 kHz, while for the Severin X_5^{S} structure, there were three band gaps in the ranges 11.02–12.76 kHz, 14.4–16.3 kHz, and 16.76–18.39 kHz. For structure X_5^{S}, the second band minimum of SPL(A) occurred at 15.44 kHz and was equal to 41.02 dB, and for the third band, it was at 17.5 kHz and was equal to 43.92 dB. Between these band gaps there was a transmission peak at 16.529 kHz and it was 82.94 dB.

Now, as a representative case, X_5^{S} has been chosen to investigate wave propagation inside the phononic structure due to the presence of a narrow peak of high transmission between the two band gaps.

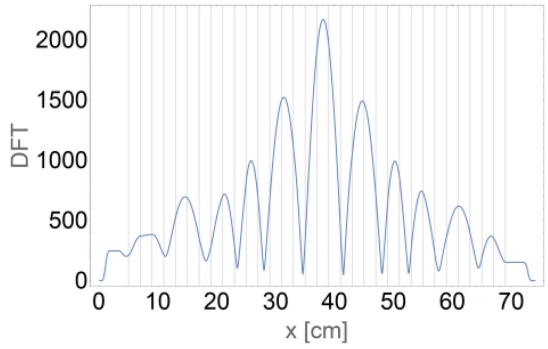

Fig. 6. The amplitude distribution obtained from DFT for the frequency of the wave source with a high transmission peak.

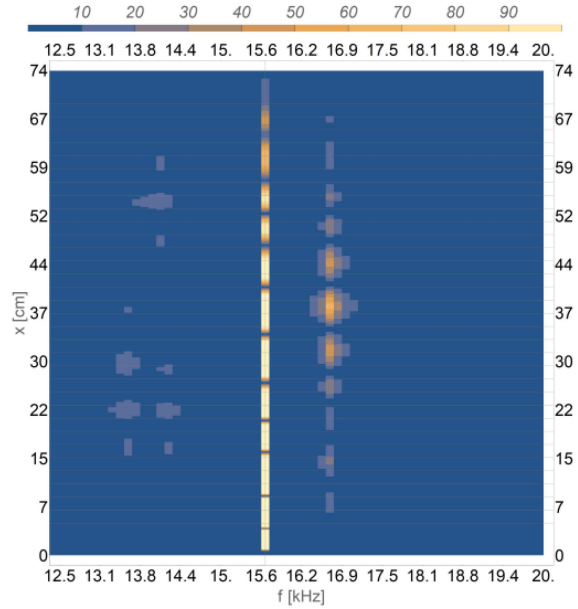

Fig. 7. The frequency distribution of the mechanical wave for the frequency of the wave source 15.5 kHz (inside the band gap).

The FDTD algorithm was used for the analysis. A soft source of the mechanical wave was used for the research, and the steps in space Δz and time Δz connected by Courant's condition were 1 mm and 2×10^{-7} s, respectively. The wave propagation time was 8×10^{-3} s. The extinction of the wave at the simulation edge was performed with the use of the PML boundary conditions.

Based on the research, time series of pressure changes in each point of the analyzed space were obtained. For each of them, a discrete Fourier transform was performed, which allowed to know the frequency distribution inside the structure for the given frequency values of the mechanical wave source. First, wave propagation analysis was performed for the transmission peak frequency of 16.5 kHz (see Figs. 4–6). Perpendicular to the x axis, the boundaries of the layers of the analyzed

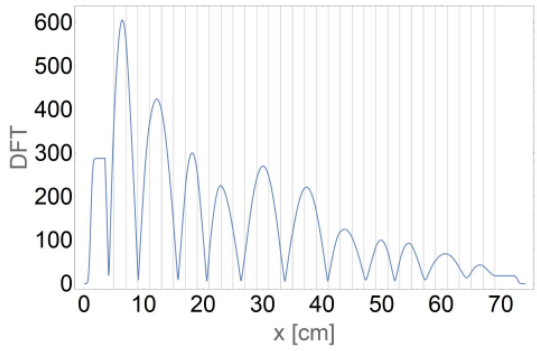

Fig. 8. Amplitude distribution for the frequency 15.5 kHz obtained from DFT for the frequency of the wave source inside the band gap.

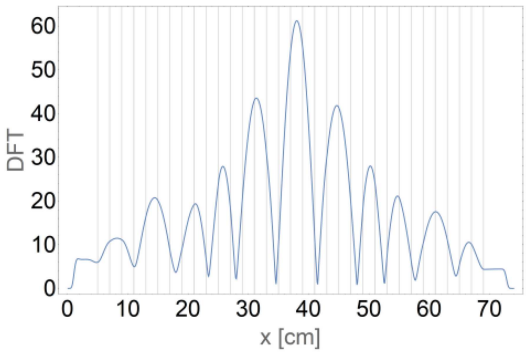

Fig. 9. Amplitude distribution for the frequency 16.5 kHz.

structure are marked. Figure 4 shows the frequency distribution of the propagating waves over the full range of acoustic frequencies, while Fig. 5 shows a narrower range around the wave source. The distribution of amplitudes inside the analyzed phononic structure is shown in Fig. 6. As can be seen in Figs. 4–6, for the source frequency corresponding to the high transmission peak, no additional spectral components appear. The frequency components around the source frequency shown in Fig. 5 result from the leakage phenomenon characteristic of the DFT method. In the wave amplitude structure in Fig. 6, nodes and antinodes characteristic for a standing wave are visible. The highest wave amplitude for the source in the high transmission peak is in the center of the analyzed structure.

In Figs. 7–11, the source of the mechanical wave was for the frequency of 15.5 kHz which was inside the band gap. As it was observed (Fig. 8), the amplitudes for the source frequencies in the band gap decreased as the wave propagated deeper into the structure. However, in the frequency distribution inside the structure (Fig. 7), component frequencies appeared at the edges of the band gap. Figure 9 shows the amplitude distribution for the frequency 16.5 kHz. Note that it has the same

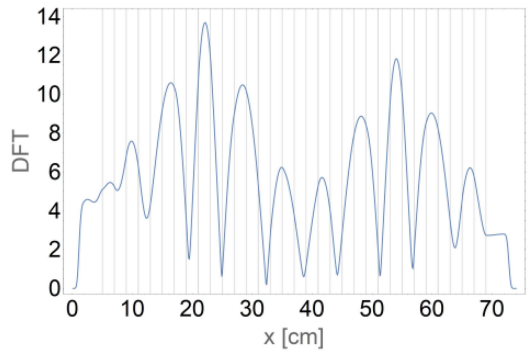

Fig. 10. Amplitude distribution for the frequency 14 kHz.

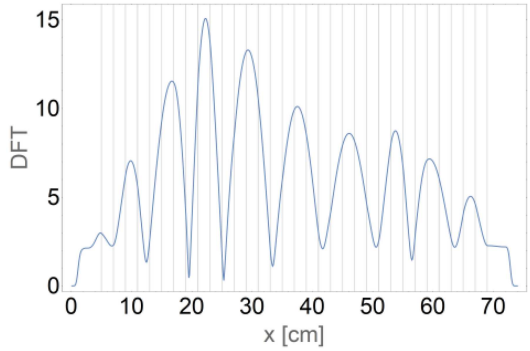

Fig. 11. Amplitude distribution for the frequency 13.375 kHz.

characteristics as the distribution in Fig. 6, but with much smaller amplitudes. Figures 10 and 11 show the amplitude distributions for the frequencies 14 kHz and 13.375 kHz, respectively. On all amplitude distributions, one can observe the formation of standing waves and clear amplitude maxima, where for the frequency 16.5 kHz there is one main maximum in the center of the structure. Similarly, for the frequency of 13.375 kHz there is a single maximum but shifted towards the wave source, while for the frequency of 14 kHz there are two amplitude maxima.

6. Conclusions

As part of the research, the properties of multilayer structures modeled with the use of the TMM and FDTD algorithms and made of PLA and water were analyzed. These structures can be used as band filters aimed at eliminating selected frequency components in the transmission spectrum due to the occurrence of the phononic band gap phenomenon. As shown, the lack of ordering of the material distribution in the structure influenced the occurrence of the band gap in the lower frequency ranges.

The conducted research on the propagation of mechanical waves inside the phononic structure showed the existence of standing waves of significant amplitudes.

The appearance of additional frequency components at the band gap boundaries inside the phononic structure was shown if the wave source had a frequency within the band gap. For the source frequency in the high transmission peak, there were no additional spectral components.

References

[1] I. Kriegel, F. Scotognella, *Physica E* **85**, 34 (2017).

[2] S. Villa-Arango, R. Torres, P.A. Kyriacou, R. Lucklum, *Measurement* **102**, 20 (2017).

[3] C.J. Rupp, M.L. Dunn, K. Maute, *Appl. Phys. Lett.* **96**, 111902 (2010).

[4] Y. Pennec, B. Djafari-Rouhani, J.O. Vasseur, A. Khelif, P. A. Deymier, *Phys. Rev. E* **69**, 046608 (2004).

[5] M. Kafesaki, M.M. Sigalas, N. García, *Phys. Rev. Lett.* **85**, 4044 (2000).

[6] X. Zhang, Z. Liu, *Nat. Mater.* **7**, 435 (2008).

[7] R.H. Olsson, I.F. El-Kady, M.F. Su, M.R. Tuck, J.G. Fleming, *Sens. Actuators A Phys.* **145–146**, 87 (2008).

[8] J. Wen, D. Yu, L. Cai, X. Wen, *J. Phys. D: Appl. Phys.* **42**, 115417 (2009).

[9] B. Morvan, A. Tinel, J.O. Vasseur, R. Sainidou, P. Rembert, A.-C. Hladky-Hennion, N. Swinteck, P.A. Deymier, *J. Appl. Phys.* **116**, 214901 (2014).

[10] A. Khelif, A. Choujaa, S. Benchabane, B. Djafari-Rouhani, V. Laude, *Appl. Phys. Lett.* **84**, 4400 (2004).

[11] J.V. Sanchez-Perez, C. Rubio, R. Martinez-Sala, R. Sanchez-Grandia, V. Gomez, *Appl. Phys. Lett.* **81**, 5240 (2002).

[12] S. Garus, *Rev. Chim.* **70**, 3671 (2019).

[13] X.-F. Li, X. Ni, L. Feng, M.-H. Lu, C. He, Y.-F. Chen, *Phys. Rev. Lett.* **106**, 084301 (2011).

[14] S.-H. Jo, H. Yoon, Y. C. Shin, B. D. Youn, *Int. J. Mech. Sci.*, **183**, 105833 (2020).

[15] Z. Wen, Y. Jin, P. Gao, X. Zhuang, T. Rabczuk, B. Djafari-Rouhani, *Mech. Syst. Signal Process.* **162**, 108047 (2022).

[16] S.-H. Jo, H. Yoon, Y. C. Shin, B. D. Youn, *Int. J. Mech. Sci.*, **193**, 106160 (2021).

[17] R. Martínez-Sala, J. Sancho, J.V. Sánchez, V. Gómez, J. Llinares, F. Meseguer, *Nature* **378**, 241 (1995).

[18] M.S. Kushwaha, P. Halevi, L. Dobrzynski, B. Djafari-Rouhani, *Phys. Rev. Lett.* **71**, 2022 (1993).

[19] Y. Tanaka, Y. Tomoyasu, S. Tamura, *Phys. Rev. B* **62**, 7387 (2000).

[20] Jin-Chen Hsu, Tsung-Tsong Wu, *IEEE Trans. Ultrason. Ferroelect. Freq. Contr.* **53**, 1169 (2006).

[21] G. Wang, X. Wen, J. Wen, L. Shao, Y. Liu, *Phys. Rev. Lett.* **93**, 154302 (2004).

[22] S. Garus, W. Sochacki, *J. Appl. Math. Comput. Mech.* **16**, 17 (2017).

[23] Y. Wang, W. Song, E. Sun, R. Zhang, W. Cao, *Physica E: Low-dimens. Syst. Nanostruct.* **60**, 37 (2014).

[24] D. Tarrazó-Serrano, S. Castiñeira-Ibáñez, E. Sánchez-Aparisi, A. Uris, C. Rubio, *Appl. Sci.* **8**, 2634 (2018).